Title
Cell infiltrative hydrogel fibrous scaffolds for accelerated wound healing

Authors
Zhao, Xin
Sun, Xiaoming
Yildirimer, Lara
et al.

Publication Date
2017-02-01

DOI
10.1016/j.actbio.2016.11.017

Peer reviewed

Acta Biomaterialia 49 (2017) 66–77

Contents lists available at ScienceDirect

Acta Biomaterialia

journal homepage: www.elsevier.com/locate/actabiomat

Full length article

Cell infiltrative hydrogel fibrous scaffolds for accelerated wound healing

Xin Zhao [a,d,e,1], Xiaoming Sun [h,1], Lara Yildirimer [a,1], Qi Lang [a], Zhi Yuan (William) Lin [a], Reila Zheng [a], Yuguang Zhang [h], Wenguo Cui [a,g,*], Nasim Annabi [a,f,*], Ali Khademhosseini [a,b,c,*]

[a] Biomaterials Innovation Research Center, Division of Biomedical Engineering, Department of Medicine, Brigham and Women's Hospital, Harvard Medical School, Boston, MA 02139, USA
[b] Wyss Institute for Biologically Inspired Engineering, Harvard University, Boston, MA 02115, USA
[c] Department of Physics, King Abdulaziz University, Jeddah 21569, Saudi Arabia
[d] School of Life Science and Technology, Xi'an Jiaotong University, Xi'an, Shaanxi 710049, China
[e] Bioinspired Engineering and Biomechanics Center, Xi'an Jiaotong University, Shaanxi 710049, China
[f] Department of Chemical Engineering, Northeastern University, Boston, MA 02115, USA
[g] Department of Orthopedics, The First Affiliated Hospital of Soochow University, Orthopedic Institute, Soochow University, Suzhou, Jiangsu 215006, China
[h] Department of Plastic and Reconstructive Surgery, Shanghai Ninth People's Hospital Affiliated to Shanghai Jiaotong University of Medicine, Shanghai 200011, China

ARTICLE INFO

Article history:
Received 17 June 2016
Received in revised form 21 October 2016
Accepted 3 November 2016
Available online 5 November 2016

Keywords:
Gelatin methacryloyl
Photocrosslinkable hydrogel
Water retention
Soft elasticity
Wound healing

ABSTRACT

Development of natural protein-based fibrous scaffolds with tunable physical properties and biocompatibility is highly desirable to construct three-dimensional (3D), fully cellularized scaffolds for wound healing. Herein, we demonstrated a simple and effective technique to construct electrospun 3D fibrous scaffolds for accelerated wound healing using a photocrosslinkable hydrogel based on gelatin methacryloyl (GelMA). We found that the physical properties of the photocrosslinkable hydrogel including water retention, stiffness, strength, elasticity and degradation can be tailored by changing the light exposure time. We further observed that the optimized hydrogel fibrous scaffolds which were soft and elastic could support cell adhesion, proliferation and migration into the whole scaffolds, facilitating regeneration and formation of cutaneous tissues within two weeks. Such tunable characteristics of the fibrous GelMA scaffolds distinguished them from other reported substrates developed for reconstruction of wound defects including glutaraldehyde-crosslinked gelatin or poly (lactic-*co*-glycolic acid) (PLGA), whose physical and chemical properties were difficult to modify to allow cell infiltration into the 3D scaffolds for tissue regeneration. We anticipate that the ability to become fully cellularized will make the engineered GelMA fibrous scaffolds suitable for widespread applications as skin substitutes or wound dressings.

Statement of Significance

In present study, we generate three-dimensional photocrosslinkable gelatin (GelMA)-based fibrous scaffolds with tunable physical and biological properties by using a combined photocrosslinking/electrospinning approach. The developed GelMA fibrous scaffolds can not only support cell viability and cell adhesion, but also facilitate cell migration and proliferation, accelerating regeneration and formation of cutaneous tissues. In addition, the physical properties of the engineered fibrous GelMA hydrogel including water retention capability, mechanical properties and biodegradability can be tuned to accommodate different patients' needs, making it a promising candidate for skin tissue engineering.

1. Introduction

Skin wounds may be subdivided into those caused by acute trauma, burns and surgical procedures, or those caused by long-term diseases such as diabetes. Healing of such wounds depends on an intricate interplay between cellular factors as well as the surrounding extracellular matrix (ECM) [1]. Tissue engineering strategies seek to accelerate wound healing by providing the

* Corresponding authors at: Biomaterials Innovation Research Center, Division of Biomedical Engineering, Department of Medicine, Brigham and Women's Hospital, Harvard Medical School, Boston, MA 02139, USA.
E-mail addresses: wgcui80@hotmail.com (W. Cui), n.annabi@neu.edu (N. Annabi), alik@bwh.harvard.edu (A. Khademhosseini).
[1] Co-first authors.

http://dx.doi.org/10.1016/j.actbio.2016.11.017
1742-7061/

wound bed with an artificial matrix into which cells such as dermal fibroblasts can migrate to proliferate and form new tissues. The ideal dermal substitute consists of a flexible and durable material which demonstrates biocompatibility and non-antigenicity when in contact with the wounded host tissue. The most commonly developed skin substitutes include hydrogels [2], sponges [3] and electrospun mats [4]. Electrospun substitutes exhibit several fundamental features for rapid and functional wound healing which render them superior to hydrogels or sponges. Their ECM-like nanofibrous architectures provide a high surface-to-volume ratio which not only enables maximal cell-material interactions and material-mediated signaling, but also promotes rapid hemostasis. Additionally, the nanoporous nature of these mats aids in nutrient and waste exchange whilst creating a barrier to external pathogens [5,6].

Despite these advantages, nanoporous structures limit three dimensional (3D) cellular infiltration [7]. To solve this, several attempts at increasing pore sizes of fibrous scaffolds have been made. The main methods involve the co-electrospinning of sacrificial fibers or the addition of porogens which can be leached out after electrospinning. For example, co-electrospinning of water-soluble poly (ethylene oxide) (PEO) and water-insoluble poly (ε-caprolactone) (PCL) fibers, the former of which act as the sacrificial component, resulted in increased pore sizes of the final PCL scaffolds [8]. Addition of salt particles onto the collecting plate while fibers were being electrospun and subsequent dissolution of these particles in water also resulted in increased pore sizes in a PCL based scaffold [9]. While these approaches allowed for the formation of larger pore sizes and improved cellular infiltration, they reduced the mechanical properties and dimensional stability of such mats, limiting their tissue engineering applications. It is, therefore, crucial to develop a strategy to synthesize fully cellularized, yet mechanically reliable scaffolds to feasibly regenerate damaged skin.

One such approach is to facilitate cell infiltration by tuning the physical properties of the electrospun nanofibers themselves without changing the fiber or pore diameter. It has been suggested that there is an essential link between the stiffness of a scaffold and its ability to promote cell adhesion, proliferation, infiltration, and differentiation [10–13]. Cell migration into a soft matrix has been found to be faster compared to that of a stiff scaffold [14,15]. This is because fibers with low stiffness result in recruitment of nearby fibers by active cells, which increases ligand density on cell surfaces and stimulates cell adhesion as well as associated signaling pathways, thus facilitating cell migration [13].

Electrospun fibers are commonly made of synthetic polymers with tunable mechanical and degradation properties. However, the lack of cell-recognition signals renders them less than ideal for skin regeneration applications. Biopolymers including collagen [16], gelatin [17–21], fibrinogen [22] and elastin [23] are promising scaffold materials for tissue regeneration owing to their abilities to improve cell-material interactions. Furthermore, their innate hydrophilicity renders them particularly amenable to retaining an appropriate balance of moisture in the wound bed to aid the healing process [24]. Additionally, the ability to absorb large quantities of water maintains the scaffold's mechanical compliance and elasticity, which is important for skin substitutes due to the high degree of tension experienced by skin tissues. To ensure that the structure of these hydrophilic scaffolds remains stable in aqueous environments, crosslinking is required. However, crosslinking with glutaraldehyde [25] or other agents [26] may induce toxicity or compromise the scaffold's mechanical compliance and elasticity [27]. Also, controlling mechanical, degradation, and biological properties of the electrospun protein-based scaffolds still remains a challenge. The primary amino acid sequence and the protein conformation dictate the mechanical and degradation properties of the end-proteins, neither of which may be effectively controlled [28]. The aim of this project is thus to fabricate electrospun natural protein-based fibrous scaffolds with tunable physical properties including water retention, mechanical and degradation characteristics. The engineered scaffolds should also be able to promote cell adhesion, proliferation and infiltration and thus to form a 3D, fully cellularized, ECM-like constructs to facilitate wound healing.

Here, by incorporating reactive methacryloyl groups into gelatin, we synthesized a photocrosslinkable gelatin prepolymer called GelMA. Electrospinning of the resulting polymer formed photocrosslinkable GelMA hydrogel fibers, which exhibited hydrophilicity and biocompatibility due to their protein domain as well as tunable physical properties (e.g., mechanical properties) due to their methacryloyl domain. Modification of gelatin with the reactive methacryloyl groups further introduced the spatial and temporal benefits of radical photocrosslinking, endowing the electrospun GelMA fibers with controllable physical properties required to aid wound healing. Through simple adjustment of the light exposure time, we could precisely tailor the physical properties of the resulting scaffolds including water permeability/retention, mechanics, and degradation kinetics. Such tunable features distinguished the engineered scaffolds from frequently used substrates like glutaraldehyde-crosslinked gelatin or poly (lactic-*co*-glycolic acid) (PLGA) (controls in this study). By mimicking the structure of the native ECM, GelMA scaffolds were proved to effectively aid wound regeneration by guiding cellular processes, making them ideal candidates for skin regeneration.

2. Materials and methods

2.1. Synthesis of GelMA

GelMA was synthesized using methods previously described [2]. In brief, 10.0 g of type A porcine skin gelatin (Sigma-Aldrich, St. Louis, MO) was dissolved in 100 mL Dulbecco's phosphate buffered saline (DPBS) (Invitrogen, San Diego, CA) at 60 °C under constant stirring. 8.0 mL of methacrylic anhydride was added at a rate of 0.5 mL·min^{-1}. After a 3 h reaction, 1:5 diluted DPBS was added to stop the reaction and the mixture was then subjected to dialysis (MWCO 12-14,000, Fisher Scientific) in distilled water for 1 week to remove salts as well as other small molecule impurities [29]. Then, the solution was freeze-dried for 1 week and the resultant white porous foam was stored at −80 °C until later use. ^{1}H NMR spectroscopy was used to assess the degree of methacryloyl modification; at room temperature, the spectra were obtained at 600 MHz frequency in deuterium oxide using a Varian INOVA NMR spectrometer. The degree of substitution was quantified using the method described by Hoch et al. [30]. Briefly, in each spectrum, the proton signal that belonged to aromatic amino acids (d = 7.0–7.5 ppm) was used as a reference. The area under the signal curves was integrated using proton signal from the methylene groups (d = 2.7–2.9 ppm) in the vicinities of lysine amino acid. The degree of substitution was calculated using this formula: 1-(integrated signal of lysine in GelMA/integrated signal of lysine in gelatin).

2.2. Fabrication of electrospun fibrous mats

2.2.1. Fabrication of electrospun PLGA fibers

500 mg of PLGA (50 kDa, 75:25) was completely dissolved in 1 mL of hexafluoro-2-propanol (HFIP, Sigma-aldrich, St. Louis, MO). The solution was then filled into a syringe and kept in a syringe pump attached to a high voltage device (Glassman High voltage, Inc. TX). An aluminium foil collector plate (30 cm × 30 cm square plate) was used on the anode. The working distance was

set to be 10–15 cm between the syringe tip and the collector plate, with the voltage between the source and the collector plate set at 20 kV. The solution was pumped out at 4 mL·h^{-1}, and 1 g of PLGA was used to spin each sheet.

2.2.2. Fabrication of electrospun gelatin fibers

Electrospinning of gelatin fibers used the same procedure as described above except that the electrospinning solution consisted of 100 mg of gelatin A from porcine skin in 1 mL of HFIP. After electrospinning, the gelatin was chemically crosslinked using glutaraldehyde (10 mL·500 mL^{-1} ethanol) overnight. Finally, the excessive glutaraldehyde was quenched using glycine (7.5 g·500 mL^{-1} distilled water). The electrospun mats were rinsed in distilled water 5 times for 10 min each and then air-dried overnight.

2.2.3. Fabrication of electrospun GelMA fibers

Electrospinning GelMA fibers followed the same protocol as that of gelatin fibers. The electrospun GelMA sheets were photocrosslinked by crosslinking the methacryloyl groups upon UV light exposure for different lengths of time. To prepare the photocrosslinking solution, 1.0 g of 2-hydroxy-4′-(2-hydroxy ethoxy)-2-methylpropiophenone (photo-initiator, Irgacure 2959, Sigma-Aldrich, St. Louis, MO) was added to 10 mL of ethanol in the absence of light and stirred until completely dissolved. Uncrosslinked electrospun GelMA fibers were immersed in the ethanol solution containing 10% photo-initiator for 2 h and exposed to 365 nm UV light (Blak-Ray B-100 Series high powered UV lamp (B-100A) at 10 cm working distance for 2 min (GelMA-2), 6 min (GelMA-6) and 10 min (GelMA-10), respectively. The crosslinked GelMA fibers were then washed with absolute ethanol to remove excess photo-initiator. The UV crosslinking method was similar to what was used previously by Burdick's group: UV crosslinking the electrospun Norbornene-functionalized hyaluronic acid fibers [31]. To confirm the crosslinking of the photocrosslinked electrospun GelMA fibers, the crosslinked electrospun mats were immersed in deionized water for 24 h to remove the uncrosslinked GelMA and dried in air until obtaining a constant weight. We observed that photocrosslinked GelMA fibers did not dissolve in 50 °C water whereas the uncrosslinked GelMA fibers dissolved immediately in the presence of water (see the video provided in the Supporting information). The weight of the electrospun fibrous mats before and after water immersion was measured using analytical electronic balance (Mettler Toledo AL204). The percentage of the weight of the crosslinked, undissolved GelMA after water immersion relative to the initial dry weight of the GelMA samples before water immersion (Wc%, which is correlated with the degree of crosslinking) was calculated using the following equation [32,33]:

$$Wc\% = \frac{W_W}{W_d} \times 100\% \quad (1)$$

where W_d is the initial dry weight of the photocrosslinked sample before water immersion and W_W is the dry weight of the photocrosslinked sample after water immersion for 24 h.

2.3. Physical characterization

2.3.1. Morphology

Morphology of the electrospun fibrous scaffolds before and after immersion in distilled water was examined using scanning electron microscope (SEM). After thorough rinsing, all the electrospun fibers before and after immersion in water for 24 h at 37 °C were subject to incubation in 1% osmium tetroxide, followed by dehydrations in graded ethanol series as well as drying at critical point with a Polaron E3000 critical point dryer (Quorum Technologies Inc., Guelph, ON, Canada). Sputter coating was conducted at 2.2 kV for 2 min using a Polaron SC7640 sputter coater before imaging with a Hitachi S-800 SEM (Hitachi High Technologies, Pleasanton, CA).

2.3.2. Water permeability, water retention and water vapor permeability

Electrospun scaffolds were cut to fit into 24-well plates, weighed, and then incubated in 1 mL of distilled water at 37 °C for 24 h. Scaffolds were then blotted dry, weighed and subjected to the following examinations:

i. Water permeability

The setup for permeability experiments was based on the work of Sell et al. [34]. Briefly, the scaffolds were placed into separate water-tight specimen mounts. A stop/start valve was used to facilitate turning the water on and off, and connected between the inflow tube and the specimen mount. The inflow reservoir was positioned near-horizontally at the top of the inflow tube. Once filled, the water level was maintained at 100–105 cm. The small difference of 5 cm was due to the negligible error contribution in permeability as per Darcy's Law. One h prior to water permeability experiments, electrospun scaffolds were soaked in distilled water. The thickness of the swollen scaffold was measured with a caliper. The tubing was filled with distilled water, and the fibrous scaffolds loaded into the specimen mount with a cross-sectional area of 0.7 cm^2. The initial volume on the pipette was recorded, and the valve was opened to allow free water flow. The volume of the pipette was recorded again after 5 min which was determined to be the cut-off time after which water flow decreased for all samples. Each material type was tested at least 4 times.

In accordance to Darcy's Law, permeability (k) was calculated using the formula below:

$$k = Q\eta h/Ftp \quad (2)$$

where k is the permeability of the scaffold in Darcy's units (D); Q is the volume of fluid that permeated the scaffold at time t; η is the fluid viscosity (in this case, 0.89 cp for water at 25 °C); h is the scaffold thickness; F is the cross sectional area of the scaffold that is perpendicular to fluid flow direction; p is the applied pressure head [34].

ii. Water retention

The weight of the samples before and after 24 h immersion in distilled water was recorded as W_D and W_0, respectively. Samples were then left in air at room temperature and the weight (Wt) was measured at pre-determined time points [35]. The water sorption SR at time t was calculated according to the following equation:

$$SR = \frac{W_t - W_D}{W_D} \times 100\% \quad (3)$$

iii. Water vapor permeability

To examine the water vapor permeability of the nanofibers, the dry PLGA, gelatin and GelMA nanofibers were separately stuck on the ends of 17 × 60 mm (O.D. × H) Glass Threaded Vials (Fisher, MA) containing 6 mL of DPBS. The vials were placed at 37 °C and weighed every 24 h to determine the water loss [34].

2.3.3. Tensile and cyclic testing

Tensile properties of the electrospun fibers were tested by using an Instron 5542 mechanical tester. Prior to uniaxial tensile testing, the electrospun fibrous sheets were cut into rectangular shapes (30 mm × 10 mm) and soaked in distilled water for 24 h. The sample was secured between opposing clamps which were approximately 20 mm apart from each other. For tensile testing, the

samples were stretched until failure at 10 mm·min^{-1}. For cyclic tensile testing, the sample was stretched to a maximum of 5 mm, then relaxed to its original length, at 10 cycles per minute for 30 cycles.

2.3.4. Degradation

Cut round samples of 2 cm diameter were incubated at 37 °C with 1 mL 0.02 units collagenase mL^{-1} of DPBS for a month [36]. At pre-determined time points, the DPBS was removed and the samples were washed twice with distilled water, lyophilized, and weighed. The following equation was used to calculate the percentage degradation (D%):

$$D\% = \frac{W_0 - W_t}{W_0} \times 100\% \quad (4)$$

where W_0 is the initial sample dry weight and W_t is the dry weight after time t.

2.4. Biological characterization

2.4.1. Cell culture

Minimum Essential Medium (MEM, Invitrogen, San Diego), supplemented with 10% fetal bovine serum (FBS) (Life Technologies, NY), 1% L-glutamine (Life Technologies, NY), and 1% penicillin/streptomycin (Life Technologies, NY), was used to culture skin dermal fibroblasts (BJ-6s, Lonza) at 37 °C and 5% CO_2. Cells were kept in tissue culture polystyrene (TCP) flasks and passaged 1:6 when a 70% confluence was reached.

BJ-6s cells were then seeded onto the surfaces of PLGA, gelatin, GelMA nanofibers and glass (control) at a seeding density of 5×10^4 cells·cm^{-2} for cell viability, adhesion and proliferation studies.

2.4.2. Cell viability

Cell viability was determined using Live/Dead® Viability Kit (Life Technologies, NY). Calcein AM and ethidium homodimer-1 were first diluted in DPBS at concentrations of 0.5 μL·mL^{-1} and 2 μL·mL^{-1}, respectively. At 1, 4, and 7 days, samples were washed 3× in DPBS and incubated in the mixture for 15 min at 37 °C. All samples were imaged immediately without mounting using a Zeiss fluorescence microscope (Zeiss, NY).

2.4.3. Cell adhesion

To examine cell adhesion on samples at days 1, 4, and 7, phalloidin (Alexa Fluor 488, Invitrogen, San Diego, CA) and DAPI (Sigma, St Louis, MO) were used to stain F-actin and cell nuclei, respectively, as per manufacturer's instructions. Briefly, following 3× wash in DPBS, samples were sequentially subject to 30-min fixation in 4% paraformaldehyde (PFA), 20-min permeabilization in 0.1% Triton X-100, and 45-min blocking in 1% BSA. Then the phalloidin solution (1:40 dilution in DPBS) was added followed by a 45-min incubation at 37 °C. Finally, DAPI solution (1:1000 dilution in DPBS) was added for 5-min incubation at 37 °C. Cell imaging was performed using a Zeiss fluorescence microscope; cell number and area were quantified using NIH ImageJ software.

2.4.4. Cell proliferation

Cell proliferation was evaluated using PicoGreen® DNA quantification assay (Life Technologies, NY). At each time point (0, 1, 4 and 7 days), the samples were lysed for 2 h with 500 μL of 50 μg·mL^{-1} proteinase k at 37 °C, and pelleted by centrifugation at 18,000g at 4 °C for 10 min. After removal of the supernatant, the samples were diluted in 100 μL 1×TE buffer and then incubated in dark with 100 μL PicoGreen® working solution (1:200 dilution in TE buffer) for 5 min at room temperature. 96-well plates (Thermo Fisher Scientific, Waltham, MA) were used for fluorescence measurement at excitation and emission wavelengths of 485 nm and 520 nm, respectively, using a microplate reader (Fluostar, Ortenberg, Germany). The standard curve was created by mixing 100 μL of each DNA concentration (2 μmol·L^{-1}, 200 nmol·L^{-1}, 20 nmol·L^{-1}, 2 nmol·L^{-1}, 0 nmol·L^{-1}) with 100 μL of PicoGreen® solution (1:200) in a 96-well plate and incubating at room temperature for 5 min. Fluorescence of the standard curve mixture was measured as described above.

2.5. Animal study

2.5.1. Mouse dorsal model of wound healing and ethics

80 healthy female ICR mice, weighed 35–40 g, were recruited from the Shanghai Slac Laboratory Animal Co. Ltd. (Shanghai, China). Ethical clearance was obtained beforehand from the Committee of Experimental Animal Administration of Shanghai Ninth People's Hospital Affiliated to Shanghai Jiaotong University School of Medicine. During the course of the study, animals were maintained under specific pathogen-free conditions (SPF) and fed ad libitum, while complying with the international ethics guidelines and the National Institutes of Health Guide concerning the Care and Use of Laboratory Animals.

Mouse dorsal wound model was used as previously described for wound healing study [37,38]. In brief, animals were anesthetized and operations were performed, both under sterile conditions. One circular full-thickness skin wound (8-mm diameter) was created on the back of each mouse, while normal skin (2 mm) was peeled around each wound to prevent the implanted scaffolds from being dislodged. The epidermis, dermis and perichondrium in each wound were completely excised. Mice were randomly assigned to four groups and received treatment with control (no treatment), PLGA, gelatin and GelMA-10 electrospun scaffolds, respectively. Mice were returned to their cages after recovering from anesthesia.

2.5.2. Macroscopic evaluation and wound healing rate

Wound healing was carefully monitored and mice were sacrificed 0, 7, 14, and 21 days after operation (n = 5). The wound healing rate in each group was calculated as the ratio of the area of healed wounds compared to the original area of wound.

2.5.3. Morphological analysis of the wound tissue

In each group, wounds were subject to excisions with a 5-mm margin of surrounding intact tissue and were then cut in halves. After 24 h of immersion in 4% formalin, they were embedded in paraffin, and subsequently cross-sectioned along the tissue. Finally, hematoxylin-eosin (H&E) and modified Masson's trichrome were used to stain the samples for examining re-epithelialization and collagen deposition, respectively [4].

2.5.4. qRT-PCR analysis

21 days after implantation, total RNA from the regenerated tissues was prepared using Trizol Reagent (Thermo Scientific, Waltham, MA) according to the manufacturer's instructions. RNA integrity was confirmed using optical density absorption ratio OD260 nm/OD280 nm between 1.8 and 2.0. cDNA was synthesized using RNA PCR kit protocol (Thermo Scientific, Waltham, MA). The primer sequences are shown in Table S1. In triplicates, quantitative polymerase chain reaction (qPCR) amplification was performed using SYBR Green PCR reagent system. Real-time qPCR was conducted in the following steps: initial 10-min denaturation at 95 °C and 40 cycles of PCR, each lasting for 15 s at 95 °C and then 45 s at 60 °C. Endogenous control GAPDH was used for normalization. Relative quantification was conducted by applying the previously described comparative $2^{-\Delta\Delta Ct}$ method.

2.6. Statistical analysis

All experiments had 5 replicates unless otherwise stated. In IBM SPPS Statistics 19 for Windows, ANOVA with a post hoc Dunn or Bonferroni test was used to analyze the data. $p < 0.05$ was considered statistically significant.

3. Results

Photocrosslinkable GelMA prepolymer contained 70% methacryloyl modification as demonstrated by ^{1}H NMR (Fig. 1). Electrospinning of the prepolymer solution and subsequent radiation with UV light for varying time periods resulted in the nanofibrous mats (GelMA-2 for 2 min, GelMA-6 for 6 min and GelMA-10 for 10 min radiation). The electrospun GelMA fibrous mats after light exposure did not appear to dissolve in 50 °C water whereas the uncrosslinked GelMA fibrous mats dissolved immediately in presence of water (see the video provided in the Supporting information). The percentages of the weight of the undissolved, crosslinked GelMA after 24 h water immersion relative to the initial dry weight of the GelMA samples were found to be 74.3 ± 1.0%, 90.0 ± 0.5% and 99.4 ± 0.8% for GelMA-2, GelMA-6 and GelMA-10, respectively. These results may suggest that the electropun GelMA fibrous sheet had different degree of crosslinking via varying the light exposure times, potentially resulting in different physical properties.

3.1. Physical characteristics of the electrospun fibrous scaffolds

3.1.1. Morphology

The microscopic morphology of the as-spun PLGA, gelatin and GelMA fibrous scaffolds was examined using SEM (Fig. 2A). Randomly aligned fibers were well-formed, smooth and with negligible beading, giving rise to highly porous scaffolds. The individual fiber diameter ranged from 700 to 1400 nm and there was no statistically significant difference between the PLGA, gelatin or GelMA fibers ($p > 0.05$). Additionally, increasing UV light exposure times did not influence fiber diameter in GelMA samples ($p > 0.05$). Immersion in water for 24 h (37 °C), however, did increase the diameter of electrospun gelatin and GelMA fibers to between 1200 and 2000 nm, likely due to water sorption into their hydrophilic fibers (Fig. S1). No such effect was observed for PLGA fibers due to their inherently hydrophobic nature.

3.1.2. Water permeability, water retention and water vapor permeability

Water permeability, measured as the fluid volume passed through the scaffold of specific area and thickness in time t [30], of GelMA scaffolds was negatively correlated with the UV light exposure time (Fig. 2B). GelMA-2 exhibited the highest water permeability at 1600 $L{\cdot}m^{-2}{\cdot}h^{-1}{\cdot}atm^{-1}$, followed by GelMA-6 (1030 $L{\cdot}m^{-2}{\cdot}h^{-1}{\cdot}atm^{-1}$) and GelMA-10 (430 $L{\cdot}m^{-2}{\cdot}h^{-1}{\cdot}atm^{-1}$). Water permeability of the control PLGA scaffolds was only 30 $L{\cdot}m^{-2}{\cdot}h^{-1}{\cdot}atm^{-1}$ and the control gelatin fibers demonstrated medium water permeability at 770 $L{\cdot}m^{-2}{\cdot}h^{-1}{\cdot}atm^{-1}$.

Water retention capacity, measured as the loss of absorbed water from the scaffolds in air at room temperature with time [31], increased with longer crosslinking time. GelMA-10 absorbed almost 6 times the amount of water of its dry weight and then steadily declined in weight to about 350% of the starting weight over the 10-day study period. GelMA-2, GelMA-6 and gelatin scaffolds followed a similar trend with relatively high initial water sorption abilities of approximately 500% of their original weight and a steady decline over the next 10 days due to the loss of absorbed water. The final percentage weights after 10 days were 270% (GelMA-6) and just over 200% for both GelMA-2 and gelatin. Fibrous PLGA scaffolds demonstrated a substantially reduced ability to absorb water (maximal sorption of 200%) and had lost all the absorbed water in three days.

A time-dependent increase in water vapor permeability, assessed as the amount of water evaporated from a container sealed using the fibrous mats over time [39], was shown in Fig. 2D. The vapor evaporation rate was around 14 $g{\cdot}m^{-2}{\cdot}h^{-1}$ for GelMA-2, GelMA-6 and the control gelatin scaffolds. GelMA-10 formed by using longer light exposure time displayed the lowest water vapor permeability at 11 $g{\cdot}m^{-2}{\cdot}h^{-1}$ whereas the hydropho-

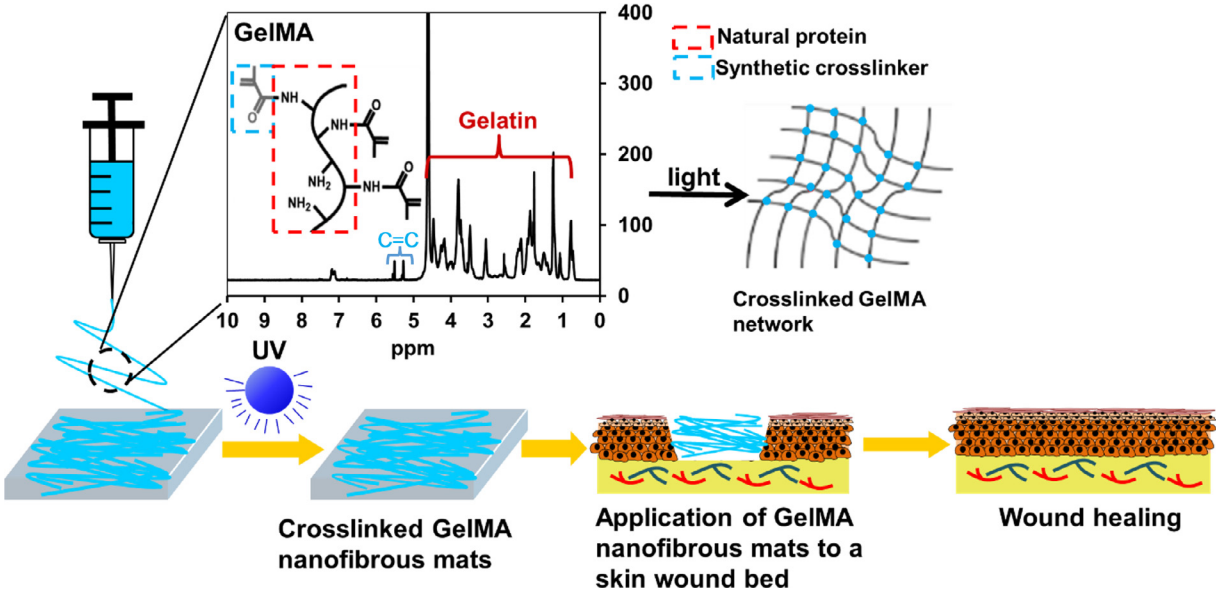

Fig. 1. Schematics for the fabrication of GelMA nanofibrous mat and its subsequent application into a wound bed. The photocrosslinkable GelMA prepolymer was electrospun onto an aluminum plate and subsequently UV light-crosslinked to obtain nanofibrous mats which were applied to wound beds to promote skin regeneration. The integrated box displays the NMR spectrum of synthesized GelMA. The gelatin component (red dashed box) was modified to contain methacryloyl groups (blue dashed box) which formed crosslinked GelMA networks upon light exposure. (For interpretation of the references to colour in this figure legend, the reader is referred to the web version of this article.)

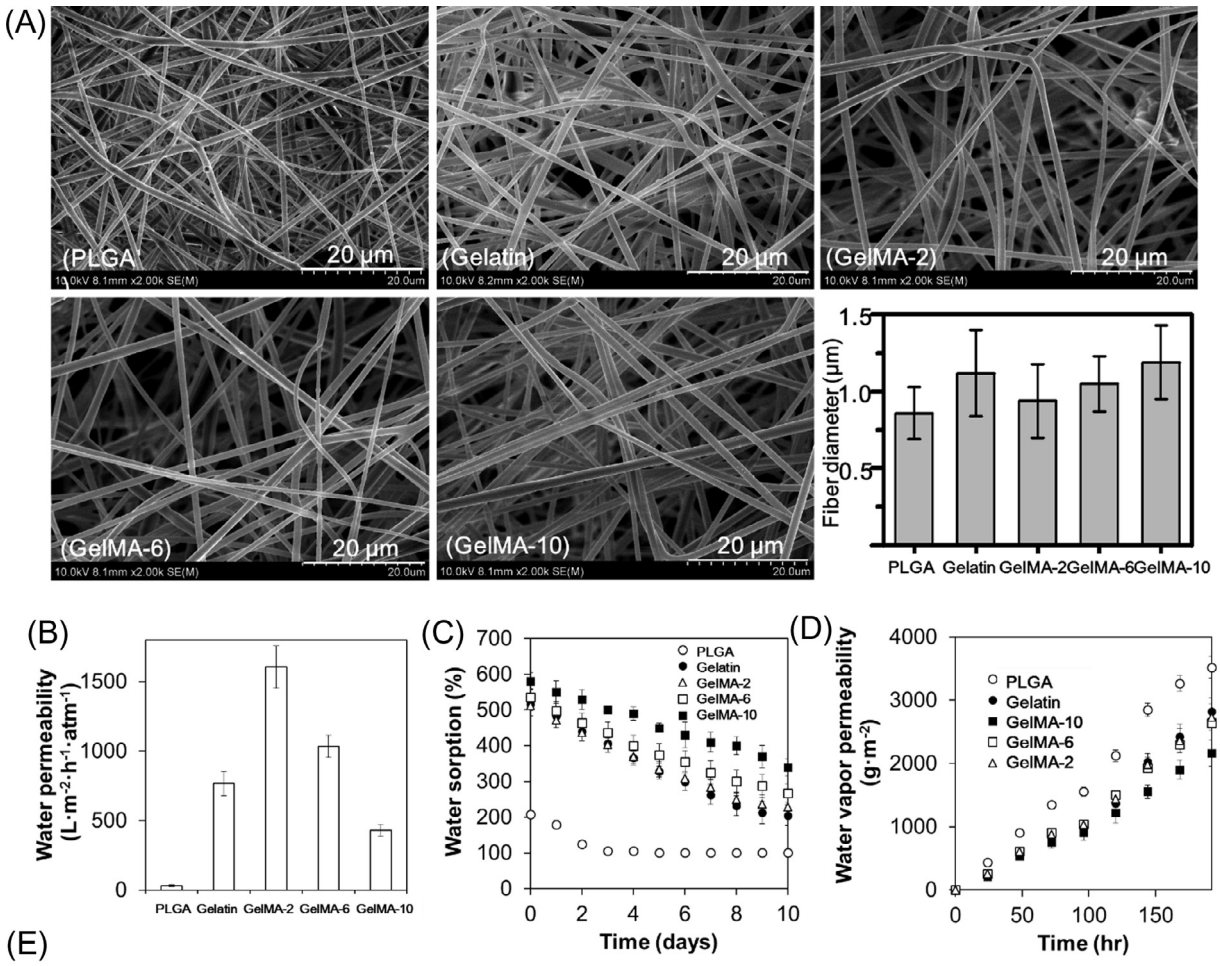

(E)

	PLGA			Gelatin			GelMA-2			GelMA-6			GelMA-10		
	k	Wr	Wv	k	Wr	Wv	k	Wr	Wv	k	Wr	Wv	k	Wr	Wv
PLGA				*	*	*	*	*	*	*	*	*	*	*	*
Gelatin	*	*	*				*			*	*		*	*	*
GelMA-1	*	*	*	*						*			*	*	*
GelMA-2	*	*	*	*	*		*						*	*	*
GelMA-3	*	*	*	*	*	*	*	*	*	*	*	*			

Fig. 2. Morphology and hydrophilicity characterization of electrospun PLGA, gelatin and GelMA scaffolds. SEM images and fiber diameter distribution (A), water permeability (B), water retention (C) and water vapor permeability (D) of electrospun PLGA, gelatin and GelMA fibers. GelMA-2, 6 and 10 represent GelMA fibers photocrosslinked by UV light radiation for 2, 6 and 10 min, respectively. Independent of the fiber material and UV light-crosslinking time, electrospun fibers displayed smooth surfaces, uniform diameters and random alignment. Water permeability of GelMA scaffolds was negatively correlated with UV light exposure time but significantly higher than that of hydrophobic PLGA scaffolds. The inverse was the case for water retention capacity which was positively correlated with longer crosslinking times. Water vapor permeability was time-dependent and inversely correlated with the crosslinking time. E) A table summarizing statistically significant difference in water permeability (k), water retention after 10 days (Wr) [14], and water vapor permeability after 192 h (Wv), between the electrospun PLGA, gelatin and GelMA fibers. *Statistical significant difference between different groups for $p < 0.05$.

bic PLGA scaffolds maintained consistently highest evaporation rates at 18 $g \cdot m^{-2} \cdot h^{-1}$.

3.1.3. Mechanical properties

All gelatin and GelMA scaffolds displayed typical stress-strain curves expected for viscoelastic materials due to the presence of gelatin segments with linear elastic behavior at low stress and non-linear region at higher stress (Fig. 3A). Young's modulus was lowest for GelMA-2 at 290 ± 40 kPa and incrementally increased to 325 ± 50 kPa and 350 ± 40 kPa for GelMA-6 and GelMA-10, respectively (Fig. 3B). Both tensile strength (Fig. 3C) and elongation at break (Fig. 3D) increased with increasing UV light exposure time (from 310 ± 20 to 360 ± 40 kPa for GelMA scaffolds and 50 ± 6% for GelMA-2, 55 ± 5% for GelMA-6, 60 ± 4% for GelMA-10, respectively). GelMA scaffolds appeared more flexible/compliant (with slightly lower Young's modulus and tensile strength) compared to the control gelatin scaffolds. GelMA-based scaffolds also exhibited a significant increase in the elongation at break with that of GelMA-10 scaffolds being comparable to the control PLGA scaffolds (66 ± 9%) whereas the PLGA scaffolds exhibited higher Young's modulus (30 ± 4 MPa) and tensile strength (37 ± 1 MPa).

Next, cyclic stress-strain data were taken to evaluate the resilience or hysteresis of the electrospun scaffolds. Different materials were loaded at different maximum strains: 1.2% for PLGA, 25% for gelatin, GelMA-2 and GelMA-6 and 30% for GelMA-10 (Fig. 3E-I). The control PLGA and gelatin scaffolds demonstrated incomplete

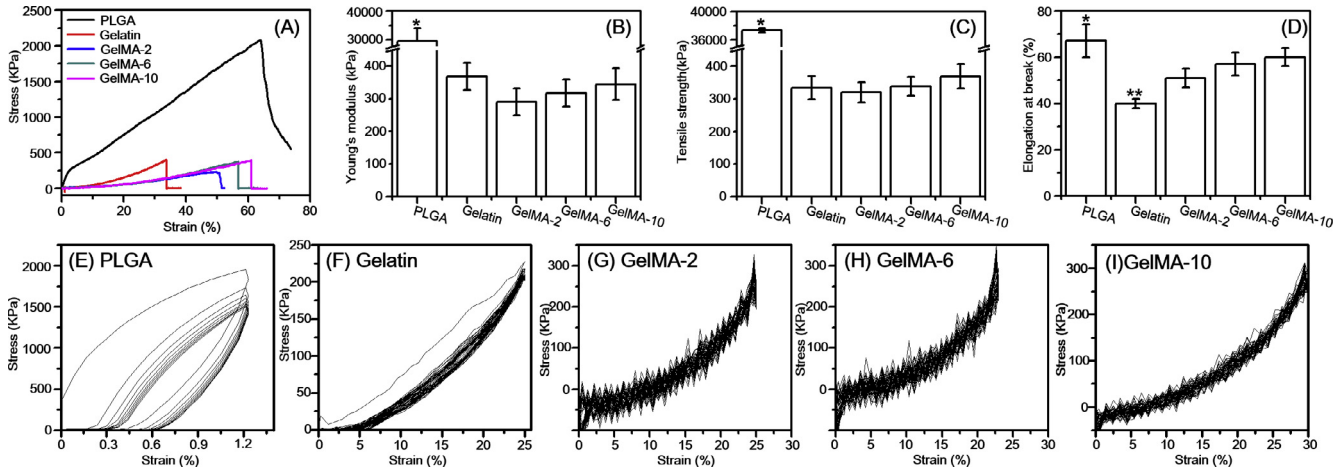

Fig. 3. Mechanical characteristics of engineered PLGA, gelatin and GelMA fibers. Representative stress-strain curves of electrospun PLGA, gelatin and GelMA scaffolds (A). Young's modulus (B), tensile strength (C) and elongation at break (D) obtained from the stress-strain curves of the electrospun PLGA, gelatin and GelMA scaffolds. An increasing trend in all three parameters was observed with increasing crosslinking time of the GelMA electrospun scaffolds, although the difference between different groups is statistically insignificant. Cyclic stress-strain curves of the electrospun PLGA (E), gelatin (F), GelMA-2 (G), GelMA-6 (H) and GelMA-10 (I) scaffolds. Scaffolds exhibited incomplete recovery from tensile strains which was most pronounced for the PLGA and gelatin controls. *Significant difference between GelMA-2, GelMA-6, GelMA-10 and the control PLGA scaffolds. **Significant difference between GelMA-2, GelMA-6, GelMA-10 and the control gelatin scaffolds.

recovery from tensile strains of 1.2% and 25%, respectively, whilst the stress-strain curves of GelMA scaffolds, overlapped and were reproducible although slight hysteresis and dissipated energy were observed during the cycle (Fig. 3G-I).

3.1.4. Degradation

Mass loss of the scaffolds was determined via immersing them in collagenase solution (0.02 units collagenase mL^{-1} of PBS) over a period of 28 days (Fig. S2). Mass loss of GelMA was found to be negatively correlated with the UV light crosslinking times. GelMA-2 exhibited the most pronounced percentage mass loss which was statistically significant compared to the mass loss of all other scaffolds ($p < 0.05$). An initial burst of mass loss of almost 15% over the first 3 days was observed, followed by a more gradual loss to 90% of the initial weight by day 28. GelMA-6 and 10 exhibited slightly higher degradation (~70%) compared to the control gelatin (~60%) scaffolds after 28 days of immersion in collagenase solution possibly due to the decreased proportion of crosslinkers compared to that in glutaraldehyde-crosslinked gelatin, making the material more hydrophilic and sensitive to degradation [40,41]. The property of biodegradation of GelMA is beneficial for skin regeneration as it can respond to the dynamic wound environment to regulate skin regeneration [42]. Additionally, the degradation product of GelMA, methacryloylated amino acid derivatives or methacrylic acid, are small molecules and relatively non-toxic, which can easily be excreted directly or after entry and exit from various metabolic pathways [43,44]. As expected, PLGA exhibited slowest degradation (8%), which may inhibit wound healing.

To conclude, the above results demonstrated that the water permeability/retention, mechanical and degradation properties of the GelMA scaffolds could be readily tuned upon variation of the light exposure time. Increase in the crosslinking time in the GelMA scaffolds resulted in increased water retention, stiffness, strength, elongation at break and elasticity but decreased water permeability and degradation possibly due to the increased crosslinking density. GelMA scaffolds with shorter crosslinking time exhibited more comparable properties with the control gelatin scaffolds although they are slightly less stiff. GelMA-10 scaffolds with longest crosslinking time demonstrated physical properties between the control gelatin and PLGA scaffolds except that they appeared less stiff than both gelatin and PLGA scaffolds. They possessed increased elongation at break compared to the control gelatin scaffolds as well as improved water permeability and water retention compared to the control PLGA scaffolds. In the following studies, GelMA-10 with the longest crosslinking time and probably highest crosslinking density was selected because it is more comparable with natural skin in terms of the capability to retain water, elasticity, strength and elongation at break.

3.2. In vitro biological properties of the electrospun scaffolds

Viability of fibroblasts was evaluated by quantifying the live and dead cells adhered to the 3D fibrous scaffolds (Fig. 4A and B). Live/dead analysis revealed that fibroblasts were viable on all three scaffolds (PLGA, gelatin, GelMA-10) with over 75% viability after 1 day and 90% after 4 and 7 days of culture. Cell proliferation was quantified using the Picogreen® DNA quantification kit. It was found that the number of cells grown on the scaffolds increased with time. On days 4 and 7, cells were most abundant on the GelMA-10 scaffolds, followed by gelatin and PLGA scaffolds (Fig. 4C, see Fig. 5 for more details). Fibroblasts grown on GelMA-10 and control gelatin surfaces appeared more elongated with higher numbers of filamentous projections compared to the cells grown on the PLGA (Fig. S3).

Cell migration was quantified using the mean migration depth, defined as the average depth of the scaffolds at which cells were detected, starting from the scaffold surface (Fig. 5A). It was found that cells seeded on the GelMA-10 scaffolds migrated deepest compared to the control PLGA or gelatin scaffolds. After 7 days of culture, the cells seeded onto the GelMA-10 scaffolds migrated to the full depth of the electrospun fibrous mats (100 μm) whereas those on the gelatin scaffolds only migrated to approximately half depth of the fibrous mats (60 μm) (Fig. 5B). PLGA showed the lowest cell migration depth (40 μm) compared to gelatin or GelMA scaffolds.

3.3. In vivo wound healing

All wounds experienced gradual healing without infection, but accelerated wound closure was found to be mediated by GelMA-10 scaffolds. On day 7 post surgery, the wounds treated using different electrospun fibrous scaffolds appeared similar. At day 14, GelMA-10 and gelatin scaffolds resulted in 80% wound closure,

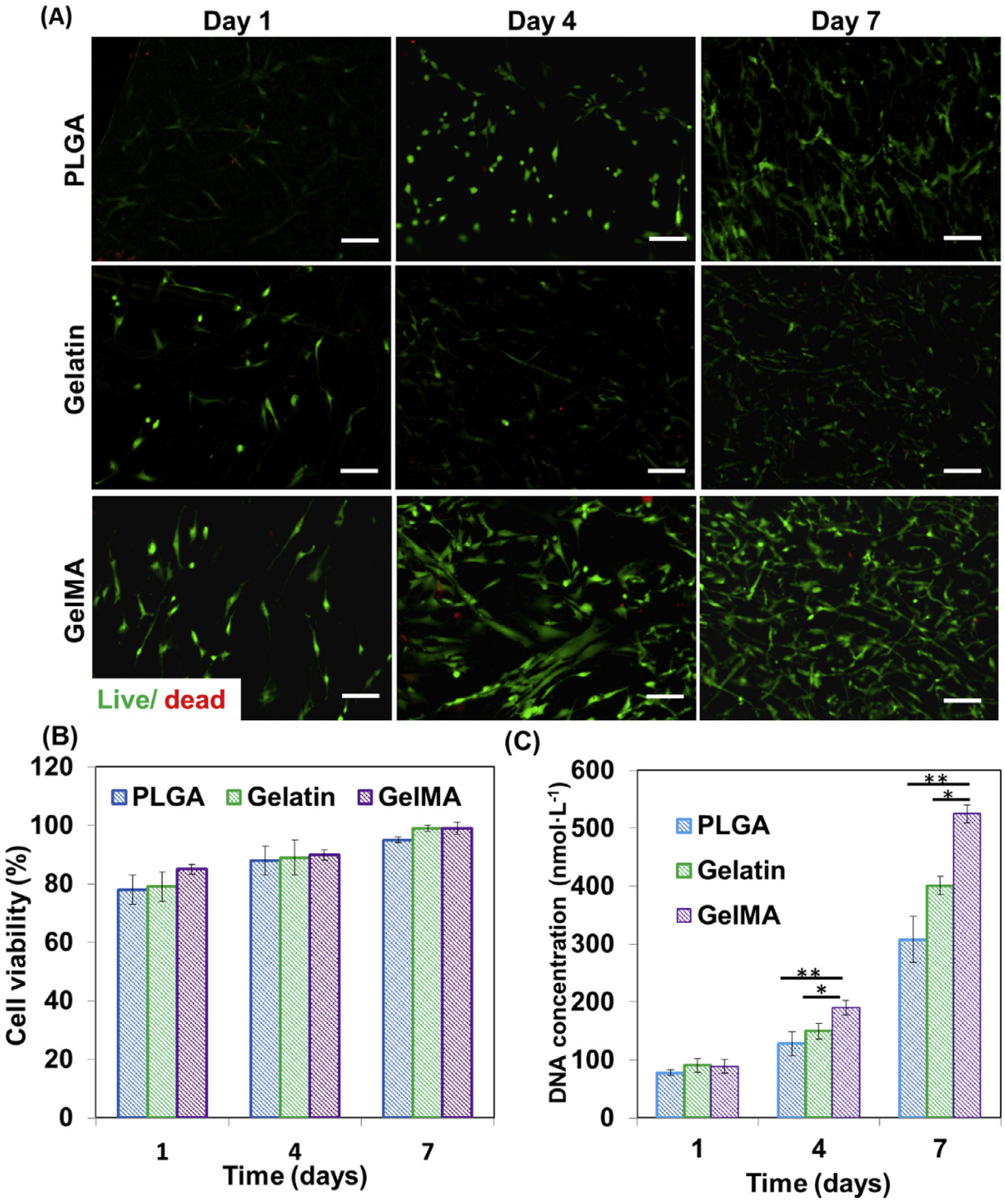

Fig. 4. *In vitro* studies on the engineered fibrous PLGA, gelatin and GelMA-10 scaffolds. Representative live/dead images based on viability test (A), quantification of cell viability (B), and cell proliferation on the electrospun scaffolds measured using PicoGreen® DNA quantification kit (C). Green fluorescent cells are living cells and red fluorescent cells indicate dead cells (scale bar = 100 μm). Most cells were alive when cultured on all scaffolds and showed a time-dependent increase in cell number. **Significant difference between GelMA-10 and PLGA scaffolds. *Significant difference between GelMA-10 and gelatin scaffolds. These results indicate that all PLGA, gelatin and GelMA-10 scaffolds have good cyto-compatibility. In particular, GelMA-10 scaffolds supported highest cell proliferation.

which was significantly greater than the 60% wound closure observed in PLGA and control groups which received no scaffolds ($p < 0.05$). After 3 weeks, those wounds closed using GelMA-10 scaffolds were completely healed although a linear scar was left (Fig. 6A). The remaining wound area relative to the original wound area was the smallest for the GelMA-10 (0%), followed by gelatin (5%), PLGA (10%) and control (15%) (Fig. S4).

3.3.1. Histologic analysis and re-epithelialization

The H&E staining images showed that the granulation tissue was present after 7 days of healing in all scaffolds (see example in Fig. 6B). After 14 days, the granulation tissue in the wound bed was gradually replaced with new tissues in the GelMA-10 scaffolds whereas it could be observed in all other samples. For gelatin and GelMA-10 samples, re-epithelialization was observed after

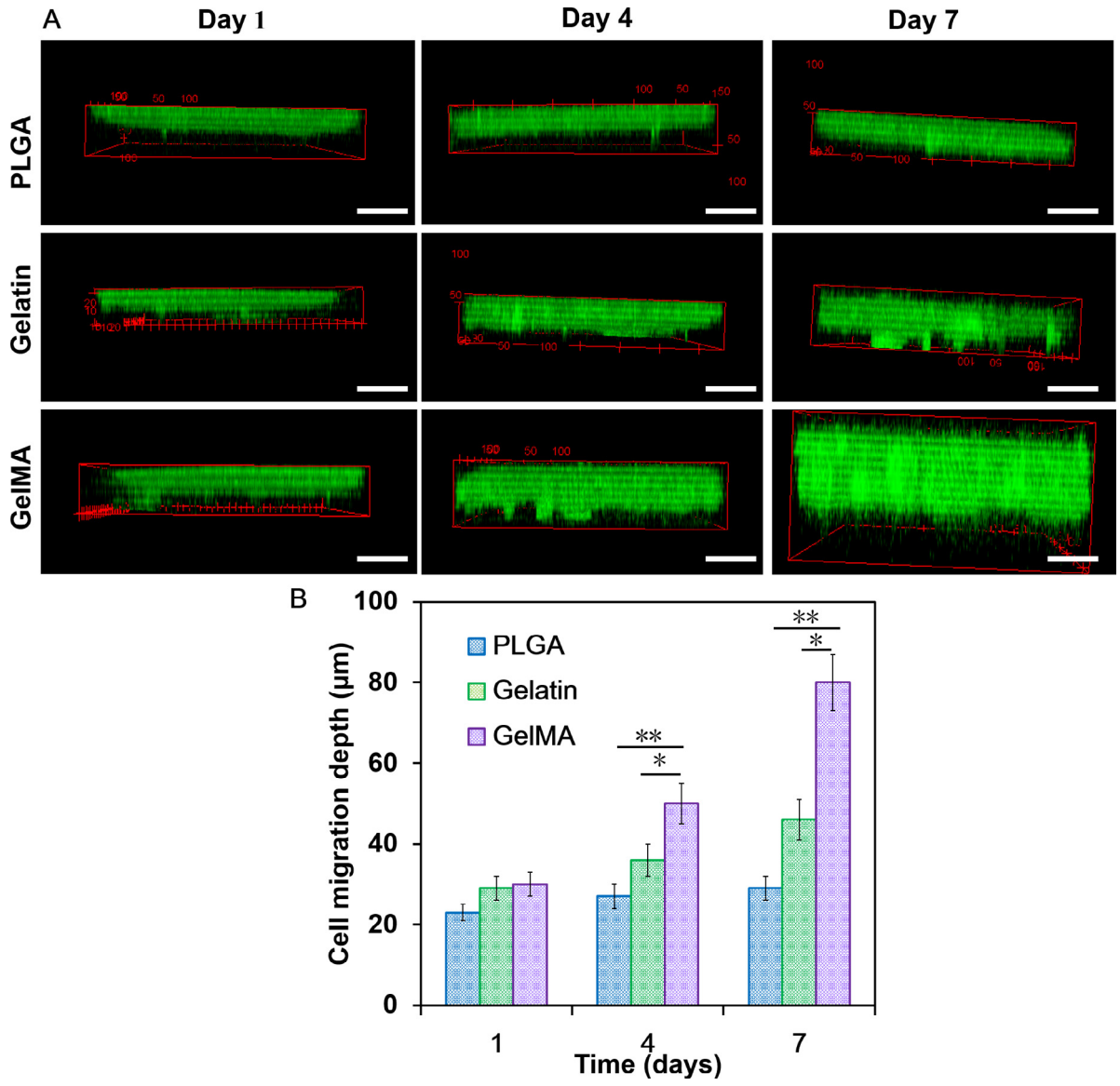

Fig. 5. Cell migration into the electrospun scaffolds. Representative images of cell migration into different scaffolds stained using phalloidin (Alexa Fluor 488) for cell filament (green) (A). Scale bar = 50 μm. Quantification of cell migration depth into different electrospun fibers over time. Cells cultured on GelMA-10 scaffolds demonstrably migrated deepest compared to the controls with cell penetration approaching 100% of the scaffold's depth at day 7 (B). **Significant difference between the GelMA-10 and PLGA scaffolds. *Significant difference between GelMA-10 and gelatin scaffolds.

14 days. After 21 days of healing, intact epidermis of 100 μm thickness was observed for both the gelatin and GelMA scaffolds whereas the resultant epidermis in PLGA or control samples appeared immature (lack of stratum corneum).

3.3.2. Collagen deposition

Masson's trichrome staining was used to highlight the collagen deposition in the wounds treated using different scaffolds. Dermal collagen fibers of PLGA and no-treatment control groups were relatively disorganized and sparse, whereas fibers of gelatin and GelMA-10 groups were bundled and arranged in a regular fashion, in particular for the GelMA-10 group. Over time, collagen fibers were increasingly deposited in all groups. On day 21 post-operatively, more collagen fibers could be observed in the samples treated with gelatin and GelMA-10 (Fig. 6C). Collagen deposition was further quantified using qPCR to evaluate the stage of tissue repair. On day 21, expression of collagen I and collagen III of the GelMA-10 group was significantly higher than other groups ($p < 0.05$). The relative expression of collagen I over collagen III of the GelMA-10 groups was significantly higher than the control and PLGA groups ($p < 0.05$) (Fig. 6D).

4. Discussion

In the present study, we demonstrated a simple and effective technique to construct 3D cell infiltrative hydrogel fibrous scaffolds for accelerated wound healing using a photocrosslinkable gelatin-based hydrogel, GelMA. Gelatin was first subjected to metharyloyl modification and electrospun into nanofibrous mats and then crosslinked upon UV exposure. Dermal fibroblasts BJ-6 cells were then cultured on the GelMA-10 nanofibrous scaffolds to examine the *in vitro* biocompatibility of the GelMA scaffolds. A murine dorsal wound healing model was used to investigate the skin regeneration potential of the GelMA-10 hydrogel fibers. PLGA and glutaraldehyde-crosslinked gelatin fibrous mats were used as

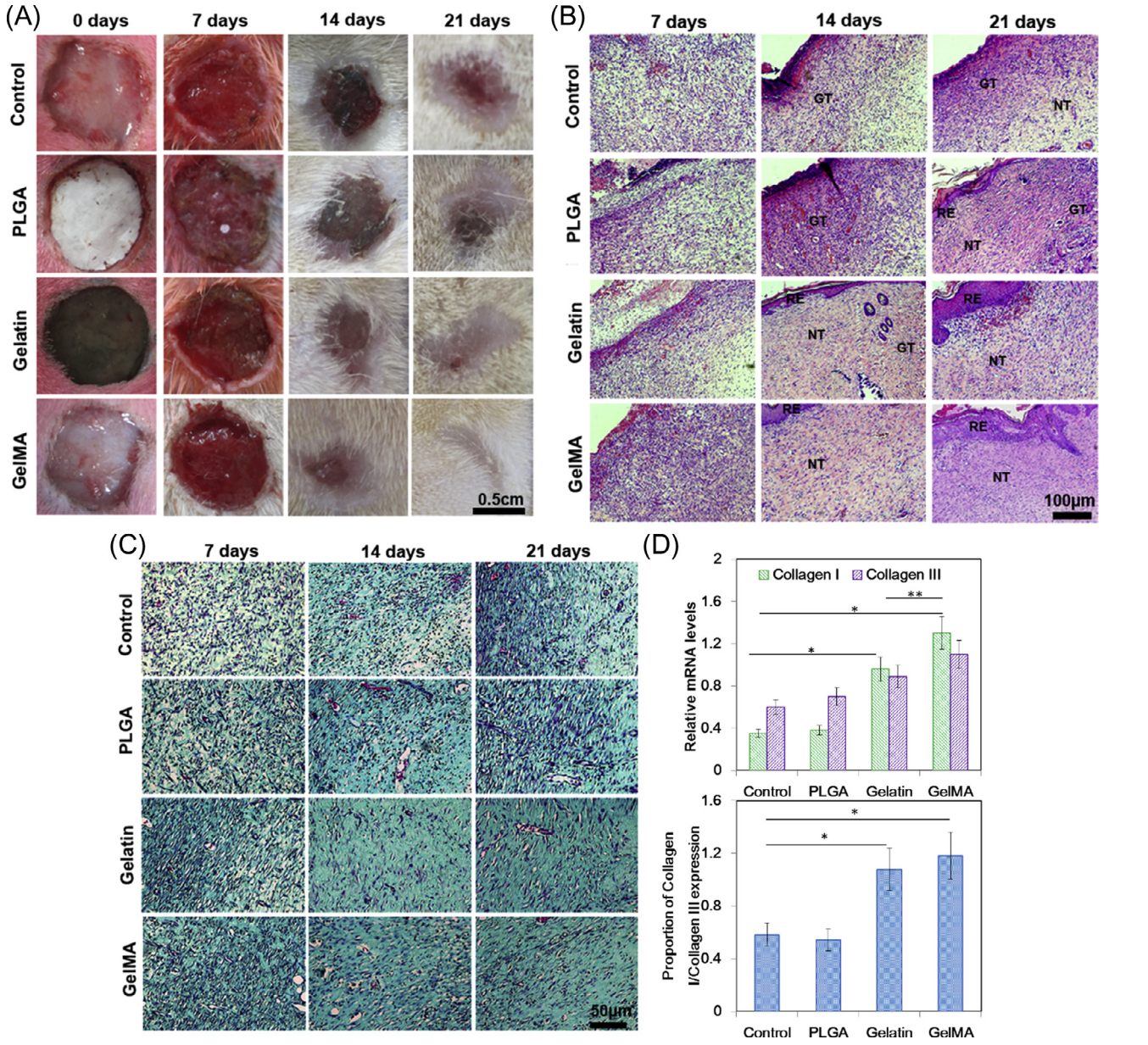

Fig. 6. *In vivo* wound healing using PLGA, gelatin and GelMA-10 scaffolds. Images of wound beds healed using different electrospun fibrous scaffolds (A). Histological appearance of wounds harvested on day 7, 14 and 21 of each group. Wounds treated with GelMA-10 scaffolds displayed faster replacement of granulation tissue with new tissues by day 14 compared to the control wounds. By day 21, only wounds treated with either GelMA-10 or gelatin scaffolds exhibited re-epithelialization, whilst untreated and PLGA-treated wounds appeared immature due to a lack of a stratum corneum layer. GT: granulation tissue; NT: neo-tissue; RE: re-epithelization (B). Masson's staining of wounds of each group harvested on day 7, 14 and 21. Collagen fibers of wounds treated with GelMA-10 scaffolds appeared bundled and regularly arranged compared to the relatively more disorganized collagen layer found in other groups (C). qRT-PCR analysis of the relative mRNA levels of Collagen I and Collagen III after 21 days of operation using different scaffolds. The relative expression of Collagen I to Collagen III increased most significantly in the GelMA-10-treated wounds, indicating optimal wound healing (D). $^{*}p < 0.05$ compared to the control group. $^{**}p < 0.05$ compared between its counterpart group.

controls to help evaluate the skin regeneration potential of the developed GelMA hydrogel fibers [45–47].

The ability of tissue engineered scaffolds to absorb significant amount of fluid whilst maintaining a moist and hydrated wound bed is of critical importance for skin regeneration [30,33]. Our results showed that, in general, water permeability decreased and water retention capacity increased with longer UV exposure times due to the increased crosslinking density which resulted in more water molecules becoming trapped within the network. Similarly, water vapor permeability was the lowest with GelMA with highest crosslinking density (crosslinked for longest time), suggesting that hydrophilic and highly crosslinked scaffolds are better able to maintain hydration of the wound bed compared to the hydrophobic PLGA controls.

Besides taking up wound exudates, skin substitutes must demonstrate suitable physical properties to accommodate different types of skin wounds. GelMA scaffolds were demonstrated to be readily tuned by changing UV light exposure times, which, if incrementally increased, resulted in increasing crosslinking density. This, in turn, was associated with higher material stiffness and strength. In our study, Young's moduli of the GelMA scaffolds fell well within the range reported in the literature for native skin which varies from 10 kPa to 50 MPa [48,49]. Whilst the stiffness and strength did indeed increase with longer light exposure time,

this did not negatively influence the scaffold's elongation at break and elasticity compared to the gelatin control. The elongation at break and elasticity is conferred by increased chain length and decreased proportion of crosslinkers (see the representative chemical structure in Fig. S5). Additionally, both the control PLGA and gelatin scaffolds demonstrated softening behaviour after repeated exposure to cyclic stress, indicating a lack of viscoelasticity. Whilst GelMA scaffolds also experienced a degree of energy dissipation as evidenced by the slight hysteresis observed during the cycles, stress-strain curves overlapped significantly more and in a reproducible fashion. The soft elasticity is hypothesized to be due to the soft chemical crosslinkers of GelMA [40,41]. GelMA-based scaffolds thus appear to have an optimal crosslinking density which grants strength whilst maintaining the elasticity required for skin substitutes [40,41].

Mechanical properties such as soft elasticity is of fundamental importance for tissue engineered skin substitutes [50] as elastic deformation of the scaffold material is known to regulate cell responses via biomechanical transduction [51–53]. Our cell seeding results demonstrated that from day 1 onwards, GelMA-10 scaffolds supported the adhesion and viability of a larger number of cells compared to the control PLGA and gelatin scaffolds and by day 7, fully cellularized 3D tissue constructs were obtained. This was aided by the capacity of cells to migrate throughout the entire depth of the GelMA-10 scaffolds, which we hypothesized was due to the GelMA fibers being less stiff than the control PLGA or gelatin fibers. Cells cultured on PLGA scaffolds showed the lowest migration depth, likely due to higher stiffness as well as a lack of cell recognition sites to guide cell migration [54]. Studies have confirmed the importance of matrix compliance with respect to cellular migratory capacities; soft 3D matrices encouraged faster cell migration compared to stiff matrices. This is postulated to be due to the ability of cells to sense their way further in a softer environment which encourages cell migration [14,15]. Also, low fiber stiffness supports active recruitment of nearby fibers by cells, which increases ligand density on the cell surface and promotes cell adhesion as well as associated signaling to ultimately facilitate cell migration [13]. It is worth noting that fibroblasts grown on GelMA-10 and gelatin surfaces appeared more elongated with higher numbers of filamentous projections compared to cells grown on PLGA scaffolds. This was likely due to the presence of cell recognition sites within ECM proteins [54].

Wound healing is a highly orchestrated event which encompasses cell adhesion, proliferation as well as migration which eventually leads to highly regulated tissue regeneration [13]. This was demonstrated in our *in vivo* skin defect models which showed that complete wound closure and re-epithelialization was only obtained with implanted GelMA-10 scaffolds. In contrast, treatment with PLGA scaffolds had almost no beneficial effect when compared to the no-treatment group with respect to wound closure. This, again, is likely due to its hydrophobic nature which prevents critical 3D cell migration [55]. Another marker for wound healing is collagen deposition. Collagen not only adds strength to the wound during healing, but also encourages cell adhesion, proliferation and differentiation. Prior to collagen deposition, the wound is held close by fibrin-fibronectin clots which, however, provide only insufficient strength [56]. Our results indicated that collagen fibers laid down on GelMA-10 scaffolds were bundled and arranged in a more regular fashion compared to gelatin, indicating a role for GelMA fibrous hydrogel scaffolds in supporting skin remodelling. This was further corroborated by the relatively higher expression of collagen I over collagen III on these scaffolds, suggesting that the collagen III produced in the proliferative phase was gradually replaced by the stronger collagen I. PLGA scaffolds as well as no-treatment control wounds, on contrast, displayed only sparse and relatively disorganized collagen fibers. In addition, ratio of collagen I over collagen III was significantly lower on these control scaffolds. Collectively, these findings indicated that the GelMA-10 scaffolds are optimal for *in vivo* wound healing.

5. Conclusions

We present a simple and effective technique to construct 3D, fully cellularized ECM-like scaffolds for accelerated wound healing using a hydrogel based on photocrosslinkable gelatin, GelMA. Due to the benefits that photocrosslinkable gelatin can provide, including tailorable mechanical and degradation properties and the ability to support cell adhesion, proliferation and migration, the resultant electrospun nanofibrous scaffolds can provide rapid regeneration and formation of cutaneous tissues within two weeks. The physical and biological properties of GelMA can be fine-tuned by altering light exposure time to accommodate different patients' needs. GelMA is a particularly promising candidate for skin tissue engineering due to its combined advantages of photopolymerizability and tunable water retention capability, mechanical properties, biodegradability as well as biocompatibility. Such unique feature is in stark contrast with other candidates such as PLGA and glutaraldehyde-crosslinked gelatin, whose properties cannot be easily modified. We envision that the GelMA hydrogel fibrous scaffolds will be suitable as wound dressings, skin substitutes, and substrate for *in vitro* skin model construction.

Acknowledgements

The authors acknowledge funding from the National Science Foundation (EFRI-1240443), IMMODGEL (602694), the National Institutes of Health (EB012597, AR057837, DE021468, HL099073, AI105024, AR063745). This work was supported in part by National Natural Science Foundation of China (51373112 and 81372073), Jiangsu Provincial Special Program of Medical Science (BL2012004), Jiangsu Provincial Clinical Orthopedic Center, the Priority Academic Program Development of Jiangsu Higher Education Institutions (PAPD).

Appendix A. Supplementary data

Supplementary data associated with this article can be found, in the online version, at http://dx.doi.org/10.1016/j.actbio.2016.11.017.

References

[1] J.E. Janis, R.K. Kwon, D.H. Lalonde, A practical guide to wound healing, Plast. Reconstr. Surg. 125 (2010) 230–244.
[2] X. Zhao, Q. Lang, L. Yildirimer, Z.Y. Lin, W. Cui, N. Annabi, K.W. Ng, M.R. Dokmeci, A.M. Ghaemmaghami, A. Khademhosseini, Photocrosslinkable gelatin hydrogel for epidermal tissue engineering, Adv. Healthc. Mater. 5 (2016) 108–118.
[3] H.M. Wang, Y.T. Chou, Z.H. Wen, Z.R. Wang, C.H. Chen, M.L. Ho, Novel biodegradable porous scaffold applied to skin regeneration, PLoS One 8 (2013) e56330.
[4] X. Sun, L. Cheng, J. Zhao, R. Jin, B. Sun, Y. Shi, L. Zhang, Y. Zhang, W. Cui, BFGF-grafted electrospun fibrous scaffolds via poly(dopamine) for skin wound healing, J. Mat. Chem. B 2 (2014) 3636–3645.
[5] R. Murugan, S. Ramakrishna, Nano-featured scaffolds for tissue engineering: a review of spinning methodologies, Tissue Eng. 12 (2006) 435–447.
[6] Q.P. Pham, U. Sharma, A.G. Mikos, Electrospinning of polymeric nanofibers for tissue engineering applications: a review, Tissue Eng. 12 (2006) 1197–1211.
[7] M.R. Ladd, T.K. Hill, J.J. Yoo, S.L. Lee, Electrospun nanofibers in tissue engineering, in: T. Lin (Ed.), Nanofibers – Production, Properties and Functional Applications, In Tech, 2011.
[8] B.M. Baker, A.O. Gee, R.B. Metter, A.S. Nathan, R.A. Marklein, J.A. Burdick, R.L. Mauck, The potential to improve cell infiltration in composite fiber-aligned electrospun scaffolds by the selective removal of sacrificial fibers, Biomaterials 29 (2008) 2348–2358.
[9] J. Nam, Y. Huang, S. Agarwal, J. Lannutti, Improved cellular infiltration in electrospun fiber via engineered porosity, Tissue Eng. 13 (2007) 2249–2257.

[10] A.J. Engler, S. Sen, H.L. Sweeney, D.E. Discher, Matrix elasticity directs stem cell lineage specification, Cell 126 (2006) 677–689.
[11] C.B. Khatiwala, S.R. Peyton, A.J. Putnam, Intrinsic mechanical properties of the extracellular matrix affect the behavior of pre-osteoblastic MC3T3-E1 cells, Am. J. Physiol. Cell Physiol. 290 (2006) 1640–1650.
[12] D.E. Discher, P. Janmey, Y.-L. Wang, Tissue cells feel and respond to the stiffness of their substrate, Science 310 (2005) 1139–1143.
[13] B.M. Baker, B. Trappmann, W.Y. Wang, M.S. Sakar, I.L. Kim, V.B. Shenoy, J.A. Burdick, C.S. Chen, Cell-mediated fibre recruitment drives extracellular matrix mechanosensing in engineered fibrillar microenvironments, Nat. Mater. 14 (2015) 1262–1268.
[14] P. Soman, J.A. Kelber, J.W. Lee, T.N. Wright, K.S. Vecchio, R.L. Klemke, S. Chen, Cancer cell migration within 3D layer-by-layer microfabricated photocrosslinked PEG scaffolds with tunable stiffness, Biomaterials 33 (2012) 7064–7070.
[15] A. Buxboim, I.L. Ivanovska, D.E. Discher, Matrix elasticity, cytoskeletal forces and physics of the nucleus: how deeply do cells 'feel' outside and in?, J Cell Sci. 123 (2010) 297–308.
[16] H.M. Powell, D.M. Supp, S.T. Boyce, Influence of electrospun collagen on wound contraction of engineered skin substitutes, Biomaterials 29 (2008) 834–843.
[17] Y.Z. Zhang, J. Venugopal, Z.M. Huang, C.T. Lim, S. Ramakrishna, Crosslinking of the electrospun gelatin nanofibers, Polymer 47 (2006) 2911–2917.
[18] K. Ulubayram, A.N. Cakar, P. Korkusuz, C. Ertan, N. Hasirci, EGF containing gelatin-based wound dressings, Biomaterials 22 (2001) 1345–1356.
[19] P.M. Neumann, B. Zur, Y. Ehrenreich, Gelatin-based sprayable foam as a skin substitute, J. Biomed. Mater. Res. 15 (1981) 9–18.
[20] T.W. Wang, H.C. Wu, Y.C. Huang, J.S. Sun, F.H. Lin, Biomimetic bilayered gelatin-chondroitin 6 sulfate-hyaluronic acid biopolymer as a scaffold for skin equivalent tissue engineering, Artif. Organs 30 (2006) 141–149.
[21] S.B. Lee, Y.H. Kim, M.S. Chong, S.H. Hong, Y.M. Lee, Study of gelatin-containing artificial skin V: fabrication of gelatin scaffolds using a salt-leaching method, Biomaterials 26 (2005) 1961–1968.
[22] R. Imani, M. Rafienia, S.H. Emami, Synthesis and characterization of glutaraldehyde-based crosslinked gelatin as a local hemostat sponge in surgery: an in vitro study, Bio-Med. Mater. Eng. 23 (2013) 211–224.
[23] E.D. Boland, J.A. Matthews, K.J. Pawlowski, D.G. Simpson, G.E. Wnek, G.L. Bowlin, Electrospinning collagen and elastin: preliminary vascular tissue engineering, Front. Biosci. 9 (2004) 1422–1432.
[24] P. Zahedi, I. Rezaeian, S.O. Ranaei-Siadat, S.H. Jafari, P. Supaphol, A review on wound dressings with an emphasis on electrospun nanofibrous polymeric bandages, Polym. Adv. Technol. 21 (2010) 77–95.
[25] S. Zhong, W.E. Teo, X. Zhu, R. Beuerman, S. Ramakrishna, L.Y. Yung, Formation of collagen-glycosaminoglycan blended nanofibrous scaffolds and their biological properties, Biomacromolecules 6 (2005) 2998–3004.
[26] S.A. Sell, P.S. Wolfe, K. Garg, J.M. McCool, I.A. Rodriguez, G.L. Bowlin, The use of natural polymers in tissue engineering: a focus on electrospun extracellular matrix analogues, Polymers 2 (2010) 522.
[27] E.A. Talman, D.R. Boughner, Glutaraldehyde fixation alters the internal shear properties of porcine aortic heart valve tissue, Ann. Thorac. Surg. 60 (1995) 369–373.
[28] R.J. Wade, E.J. Bassin, C.B. Rodell, J.A. Burdick, Protease-degradable electrospun fibrous hydrogels, Nat. Commun. 6 (2015) 6639.
[29] T. McOscar, Functionalization of Nanocellulouse Fibers for Use in Radical Reactions (PhD thesis), 2015.
[30] E. Hoch, C. Schuh, T. Hirth, G.M. Tovar, K. Borchers, Stiff gelatin hydrogels can be photo-chemically synthesized from low viscous gelatin solutions using molecularly functionalized gelatin with a high degree of methacrylation, J. Mater. Sci. Mater. Med. 23 (2012) 2607–2617.
[31] R.J. Wade, E.J. Bassin, W.M. Gramlich, J.A. Burdick, Nanofibrous hydrogels with spatially patterned biochemical signals to control cell behavior, Adv. Mater. 27 (2015) 1356–1362.
[32] A. Bigi, G. Cojazzi, S. Panzavolta, K. Rubini, N. Roveri, Mechanical and thermal properties of gelatin films at different degrees of glutaraldehyde crosslinking, Biomaterials 22 (2001) 763–768.
[33] L. Yang, C.F.C. Fitié, K. Werf, M.L. Bennink, P.J. Dijkstra, J. Feijen, Mechanical properties of single electrospun collagen type I fibers, Biomaterials 29 (2008) 955–962.
[34] S. Sell, C. Barnes, D. Simpson, G. Bowlin, Scaffold permeability as a means to determine fiber diameter and pore size of electrospun fibrinogen, J. Biomed. Mater. Res. Part A 85 (2008) 115–126.
[35] K.K. Nayak, P. Gupta, In vitro biocompatibility study of keratin/agar scaffold for tissue engineering, Int. J. Biol. Macromol. 81 (2015) 1–10.
[36] A.P. Kishan, R.M. Nezarati, C.M. Radzicki, A.L. Renfro, J.L. Robinson, M.E. Whitely, E.M. Cosgriff-Hernandez, In situ crosslinking of electrospun gelatin for improved fiber morphology retention and tunable degradation, J. Mat. Chem. B 3 (2015) 7930–7938.
[37] L. Wu, G.F. Pierce, D.A. Ladin, L.L. Zhao, D. Rogers, T.A. Mustoe, Effects of oxygen on wound responses to growth factors: Kaposi's FGF, but not basic FGF stimulates repair in ischemic wounds, Growth Factors 12 (1995) 29–35.
[38] J.L. Xie, H.N. Bian, S.H. Qi, H.D. Chen, H.D. Li, Y.B. Xu, T.Z. Li, X.S. Liu, H.Z. Liang, B.R. Xin, Y. Huan, Basic fibroblast growth factor (bFGF) alleviates the scar of the rabbit ear model in wound healing, Wound Repair Regen. 16 (2008) 576–581.
[39] Y. Shi, Y. Li, J. Wu, W. Wang, A. Dong, J. Zhang, A novel transdermal drug delivery system based on self-adhesive Janus nanofibrous film with high breathability and monodirectional water-penetration, J. Biomater. Sci. Polym. Ed. 25 (2014) 713–728.
[40] C.L. Dominique, A. Pascal, B.M. Martine, Biocompatibility of Elastomers, Polymeric Biomaterials, CRC Press, 2013, pp. 415–494.
[41] M. Szycher, A.M. Reed, Biostable polyurethane elastomers, Med. Device Tech. 3 (1992) 42–51.
[42] J. Patterson, J.A. Hubbell, Enhanced proteolytic degradation of molecularly engineered PEG hydrogels in response to MMP-1 and MMP-2, Biomaterials 31 (2010) 7836–7845.
[43] A.S. Sawhney, C.P. Pathak, J.J. Rensburg, R.C. Dunn, J.A. Hubbell, Optimization of photopolymerized bioerodible hydrogel properties for adhesion prevention, J Biomed. Mater. Res. 28 (1994) 831–838.
[44] X. Zhao, I. Olsen, H. Li, K. Gellynck, P.G. Buxton, J.C. Knowles, P.G. Buxton, J.C. Knowles, V. Salih, A.M. Young, Reactive calcium-phosphate-containing poly (ester-co-ether) methacrylate bone adhesives: chemical, mechanical and biological considerations, Acta Biomater. 6 (2010) 845–855.
[45] M. Norouzi, I. Shabani, H.H. Ahvaz, M. Soleimani, PLGA/gelatin hybrid nanofibrous scaffolds encapsulating EGF for skin regeneration, J. Biomed. Mater. Res. A 103 (2015) 2225–2235.
[46] Z.X. Meng, Y.S. Wang, C. Ma, W. Zheng, L. Li, Y.F. Zheng, Electrospinning of PLGA/gelatin randomly-oriented and aligned nanofibers as potential scaffold in tissue engineering, Mat. Sci. Eng. C 30 (2010) 1204–1210.
[47] H.M. Powell, S.T. Boyce, Fiber density of electrospun gelatin scaffolds regulates morphogenesis of dermal-epidermal skin substitutes, J. Biomed. Mater. Res. A 84 (2008) 1078–1086.
[48] P.G. Agache, C. Monneur, J.L. Leveque, J. De Rigal, Mechanical properties and Young's modulus of human skin in vivo, Arch. Dermatol. Res. 269 (3) (1980) 221–232.
[49] G. Jin, M.P. Prabhakaran, S. Ramakrishna, Stem cell differentiation to epidermal lineages on electrospun nanofibrous substrates for skin tissue engineering, Acta Biomater. 7 (2011) 3113–3122.
[50] T.L. Yang, Chitin-based materials in tissue engineering: applications in soft tissue and epithelial organ, Int. J. Mol. Sci. 12 (2011) 1936–1963.
[51] D.Y. Li, B. Brooke, E.C. Davis, R.P. Mecham, L.K. Sorensen, B.B. Boak, E. Eichwald, M.T. Keating, Elastin is an essential determinant of arterial morphogenesis, Nature 393 (1998) 276–280.
[52] G. Faury, S. Garnier, A.S. Weiss, J. Wallach, T. Fulop Jr., M.P. Jacob, R.P. Mecham, L. Robert, J. Verdetti, Action of tropoelastin and synthetic elastin sequences on vascular tone and on free Ca2+ level in human vascular endothelial cells, Circ. Res. 82 (1998) 328–336.
[53] D.Y. Li, G. Faury, D.G. Taylor, E.C. Davis, W.A. Boyle, R.P. Mecham, P. Stenzel, B. Boak, M.T. Keating, Novel arterial pathology in mice and humans hemizygous for elastin, J Clin. Invest. 102 (1998) 1783–1787.
[54] T.S. Panetti, D.F. Hannah, C. Avraamides, J.P. Gaughan, C. Marcinkiewicz, A. Huttenlocher, D.F. Mosher, Extracellular matrix molecules regulate endothelial cell migration stimulated by lysophosphatidic acid, J. Thromb. Haemost. 2 (2004) 1645–1656.
[55] D.R. Griffin, W.M. Weaver, P.O. Scumpia, D. Di Carlo, T. Segura, Accelerated wound healing by injectable microporous gel scaffolds assembled from annealed building blocks, Nat. Mater. 14 (2015) 737–744.
[56] G. Song, D.T. Nguyen, G. Pietramaggiori, S. Scherer, B. Chen, Q. Zhan, R. Ogawa, I.V. Yannas, A.J. Wagers, D.P. Orgill, G.F. Murphy, Use of the parabiotic model in studies of cutaneous wound healing to define the participation of circulating cells, Wound Repair Regen. 18 (2010) 426–432.